Hindawi Publishing Corporation
Journal of Nanotechnology
Volume 2013, Article ID 736478, 9 pages
http://dx.doi.org/10.1155/2013/736478

Research Article

Improving Passivation Process of Si Nanocrystals Embedded in SiO_2 Using Metal Ion Implantation

Jhovani Bornacelli, Jorge Alejandro Reyes Esqueda, Luis Rodríguez Fernández, and Alicia Oliver

Instituto de Física, Universidad Nacional Autónoma de México, 04510 México, DF, Mexico

Correspondence should be addressed to Alicia Oliver; oliver@fisica.unam.mx

Received 30 October 2012; Accepted 16 December 2012

Academic Editor: A. M. Rao

Copyright © 2013 Jhovani Bornacelli et al. This is an open access article distributed under the Creative Commons Attribution License, which permits unrestricted use, distribution, and reproduction in any medium, provided the original work is properly cited.

We studied the photoluminescence (PL) of Si nanocrystals (Si-NCs) embedded in SiO_2 obtained by ion implantation at MeV energy. The Si-NCs are formed at high depth (1-2 μm) inside the SiO_2 achieving a robust and better protected system. After metal ion implantation (Ag or Au), and a subsequent thermal annealing at 600°C under hydrogen-containing atmosphere, the PL signal exhibits a noticeable increase. The ion metal implantation was done at energies such that its distribution inside the silica does not overlap with the previously implanted Si ion . Under proper annealing Ag or Au nanoparticles (NPs) could be nucleated, and the PL signal from Si-NCs could increase due to plasmonic interactions. However, the ion-metal-implantation-induced damage can enhance the amount of hydrogen, or nitrogen, that diffuses into the SiO_2 matrix. As a result, the surface defects on Si-NCs can be better passivated, and consequently, the PL of the system is intensified. We have selected different atmospheres (air, H_2/N_2 and Ar) to study the relevance of these annealing gases on the final PL from Si-NCs after metal ion implantation. Studies of PL and time-resolved PL indicate that passivation process of surface defects on Si-NCs is more effective when it is assisted by ion metal implantation.

1. Introduction

A common process used to obtain silicon nanocrystals (Si-NCs) involves ion implantation of Si ions into silica matrix followed by thermal annealing. Precipitation of excess Si in SiO_2 typically requires temperatures in the range 1000–1100°C for 1 h and produces Si-NCs with diameters between 3 to 7 nm [1, 2]. Si-NCs exhibit a strong room temperature photoluminescence (PL) as a direct consequence of their small size, but nonradiative surface defects, as P_b defect, compete with radiative process [3–6]. SiO_2 is an appropriate matrix for Si-NCs since it can passivate some dangling bonds that can cause nonradiative transitions. However, a better control of surface defects on Si-NCs is valuable for light-emitting applications [3, 6, 7]. Annealing in molecular hydrogen can reduce the high concentration of surface defects, and then luminescence intensity from Si-NCs significatively increases [2–8]. It has been reported that a sample containing Si-NCs and passivated at 510°C in molecular hydrogen can increase its photoluminescence signal by a factor of seven [4].

Si ion implantation is typically done at energies in the range of 35–400 KeV so the formed nanocrystals are inside the silica matrix but near its surface at a distance not exceeding 1 μm [1–4, 6, 8–11]. So molecular hydrogen can diffuse until the region where the Si-NCs were formed and P_b defects can be passivated. The closer to the Si-NCs surface are the better passivation process will be, but at the expense of greater protection and robustness of the sample. Other gases as O_2 and N_2 have been used to passivated P_b defects on Si-NCs. However, annealing in N_2 has been shown to have a negligible effect on luminescence properties of Si-NCs [8, 9]. Annealing in N_2 at temperature in the range 750°C to 1100°C can contribute to the passivation of the Si-NCs surface and consequently the PL intensity increases [9]. But at nitrogen high concentration there is a size reduction of Si-NCs by oxynitridation at their surface. As a consequence, the PL spectra could be blue shifted, and if the size is strongly

Table 1: Si-NCs preparation at 1.5 MeV.

Sample	Implantation	Steps thermal treatment	Thermal treatment
A	Si	1	1100°C for 1 h in RA
	—	—	
B	Si	1	1100°C for 1 h in Ar
	—	2	510°C for 1 h in RA
A1	Si	1	1100°C for 1 h in RA
	—	2	1100°C for 1 h in RA
A2	Si	1	1100°C for 1 h in RA
	—	2	1100°C for 2 h in RA

reduced the PL intensity can decrease [9]. Another process used to reduce the surface defects concentration on Si-NCs is known as alneal [4]. In this method, before annealing in forming gas (5% H_2 in N_2), an Al thin film (100 nm) is grown onto the surface of the substrate containing the Si-NCs. Atomic hydrogen can be generated within the oxide layer and it easily saturate the dangling bonds. This method has been showed to result in a more efficient passivation process and consequently in an increase of the PL signal by a factor of two, compared to a sample annealed in molecular hydrogen [4].

The passivation process appears to have a limit; that is, the PL intensity from Si-NCs does not increase further, even when the sample is annealed for more than 1 h, and up to 16 h in forming gas, at annealing temperatures ranging between 300 to 600°C [4, 6, 8]. This limit could be understood considering that there are a finite number of Si-NCs and also a finite number of surface defects on them. In addition to this, even though the silica matrix protects the system of Si-NCs from environment effects, it is a barrier to overcome in order to saturate the dangling bonds in the Si-NCs surface. This fact imposes a limit to the PL signal enhancement.

In this work, we synthesize a system of Si-NCs embedded in Silica by ion implantation at 1.5 MeV. At this energy, the Si-NCs are formed in a depth region inside the silica matrix. SRIM simulation shows that the Si ion implantation distribution in silica has a maximum in 1.7 μm, in the range of 1-2 μm under the silica surface. This deep Si ion implantation allows to obtain a more robust sample well protected from external damage and environmental contamination. A device with these properties is a good candidate for optoelectronics applications. However, the amount of hydrogen which can diffuse into the silica matrix of these samples is more limited than the samples obtained by the traditional ion implantation. In this case, the Si-NCs are at a depth greater than 1 μm, so the matrix barrier imposed to the hydrogen diffusion is higher. Once the Si-NCs are synthesized by ion implantation at MeV energy, in order to overcome that barrier, the silica matrix is again irradiated with Ag ions (or Au ions). This ion irradiation is carried out at energies which make, both, metal and Si ions distributions, very close to each other but without overlapping. This slight separation between the two distributions of the implanted ions is very important to preserve the PL emission from Si-NCs. It has been observed that ion metal implantation could quench the PL from Si-NCs [12, 13]. On the other hand, the PL signal from Si-NCs can be enhanced by the localized plasmon interaction induced by the nucleation of metal nanoparticles under controlled annealing [14, 15]. Then, the enhancement of the PL emission from the integrated system studied in this work could have two contributions. One of them could take place as a result of the ion-metal-implantation induced damage that could increase the amount of hydrogen that diffuses into the silica matrix. The other could be the presence of metal NPs formed inside the silica matrix that may result in a plasmonic interaction between Si-NCs and metal nanoparticles, increasing even more the final photoluminescence of the system.

2. Experiment

(A) Si-NCs Preparation. Silica glass plates (20 × 20 × 1 mm) were implanted at room temperature with 1.5 MeV Si^{+2} ions at fluence of 2.5×10^{17} ions/cm^2, using the 3 MV Tandem accelerator (NEC 9SDH-2 Pelletron) facility at the Instituto de Física of the Universidad Nacional Autónoma de México (IFUNAM). After implantation, we explored two methods of nucleation and growth of Si nanocrystals. One sample was thermally annealed in a reducing atmosphere (RA) consisting of 50% N_2 and 50% H_2 at 1100°C for 1 h (Method A), in order to nucleate the Si NCs from the supersaturated solution. A similar method was used by Wilkinson and Elliman [8] but in a system with Si ions implanted at 100 keV. A second piece was annealed in Ar gas at 1100°C for 1 h and then passivated at 510°C in RA for 1 h (Method B). The last method is commonly used in other works but in samples implanted with Si ions at low energy (35–200 KeV) [1, 4, 6, 8–10, 16]. In the following, samples prepared by method A or B will be labeled sample A or sample B, respectively. On the other hand, a two-sample set was prepared according to method A, one of them was annealed again for 1 h (sample A1) and the other for 2 h (sample A2), in RA at 1100°C in order to compare the effect of annealing for more than 1 h (see Table 1).

(B) Silica Matrix with Si-NCs Implanted with Ag Ion. Once the Si-NCs have been formed inside the matrix (by Method A), the sample was cut into pieces. One of the pieces was implanted at room temperature with Ag^{+2} ions at energy of 1 MeV and a fluence of 6×10^{16} ions/cm^2. After the Ag implantation, the samples were again thermally annealed in RA at 600°C for 1 h (Sample A(Ag)). At this temperature, Ag nanoparticles (Ag-NPs) were formed. The Ag-NPs produced in this way have an average diameter of 6 nm [17]. At the end of this process, we obtained two kinds of samples, one having only Si NCs embedded (Sample A), and a second one with Si NCs and Ag NPs embedded into the silica matrix (Sample A(Ag)).

Monte Carlo simulations were performed with the SRIM program to determine the Gaussian depth distribution of the implanted ions: the atoms of the implanted Ag were distributed in the range of 110–830 nm, with its maximum at 480 nm, while for Si the atoms were in the range of 300–2200 nm, with its maximum at 1700 nm.

Table 2: Resume of the process to obtain the samples studied in this work. Si, Ag, and Au implantations were done at 1.5, 1.0, and 1.9 MeV, respectively.

Sample	Implantation	Steps thermal treatment	Thermal treatment
A(Ag)*	Ag	1	600°C for 1 h in RA
A2(Ag)-1*	Ag	1	600°C for 1 h in RA
A2(Ag)-2*	Ag	1	600°C for 1 h in Ar
A(Au)-1*	Au	1	600°C for 1 h in RA
A(Au)-2*	Au	1	1100°C for 1 h in RA
A(Au)-3*	Au	1	1100°C for 1 h in Air

*The samples with metal ion implantation were previously prepared as a sample A or A2 (see Table 1) as indicated in the first letter and number in its label.

In order to compare the effect of the Ag-NPs and the annealing environment, over the final PL intensity of the integrated system, the sample A2 with Si-NCs in SiO_2 was implanted with Ag^{+2} ions at the same conditions explained previously. The sample was cut into two pieces and was thermally annealed at 600°C for 1 h but one of them in RA (Sample A2(Ag)-1) and the other in Ar gas (Sample A2(Ag)-2, see Table 2).

(C) Silica Matrix with Si-NCs Implanted with Au Ion. Another sample set containing Si-NCs prepared by method A, as explained before, was implanted with Au^{+2} ions at energy of 1.9 MeV and a fluence of 6×10^{16} ions/cm^2. The sample was cut into small pieces. One of these samples was heated in RA at 600°C for 1 h (Sample A(Au)-1). Other two pieces were also heated at 1100°C, one in RA (Sample A(Au)-2) and the other in air (Sample A(Au)-3). Au nanoparticles (Au-NPs) may be formed in the sample only by heating at 1100°C in air. The Au-implanted ions were distributed in the range 160–820 nm with its maximum at 502 nm, according to the SRIM simulation.

The ion range of the Ag and Au implantations was corroborated by means of Rutherford backscattering spectrometry (RBS) using a 2 MeV He^+ beam. We use the RUMP code to calculate the concentration profile of the implanted ions.

Table 2 shows a resume of the samples studied in this work.

(D) PL, Time-Resolved PL, and Optical Absorption. Photoluminescence (PL) measurements were performed at room temperature at excitation wavelengths of 250, 355, and 420 nm using ps pulses, at a frequency repetition rate of 10 Hz, from a combined laser system PL2143A + PG401/SH by EKSPLA, at the Nonlinear Optics Laboratory of IFUNAM. In this range of excitation wavelengths, all the Si-NCs of the sample may absorb light and then contribute to the PL signal, which was collected by a 1000 microns optical fiber and detected by an Ocean Optics USB2000+ spectrometer. Some PL spectra were obtained using 250 nm as excitation wavelength to see a possible PL from defects produced in the silica matrix after ion implantation [18–20]. Photoluminescence measurements versus excitation pump pulse fluence were carried out at 355 nm and 420 nm. For each of these excitation wavelengths, neutral optical densities were used to control the incident irradiance over the samples. The peak signal of the PL spectrum was acquired every 1 s over a total integration time of 3 min, for each of the excitation pump pulse fluences. All the measurements were performed by keeping the illumination area over the sample constant, using a mechanical aperture. The time-resolved PL was measured with excitation wavelength of 355 nm. The emerging PL was resolved with an Acton Series SP2300 monochromator and detected with a Hamamatsu H10721-20 photomultiplier module, connected to a digital oscilloscope where the microsecond PL signal could be visualized over a few hundred μs. Emission decay lifetimes were extracted by the least-square fitting of a stretched exponential. The PL decay was investigated at a wavelength set around peak intensity of PL spectrum. The optical absorption of all the samples was measured by means of a Varian Cary 5000 UV-VIS spectrophotometer.

3. Results and Discussion

Figure 1(a) shows a broad PL emission, which is a characteristic emission from Si-NCs, and is observed for both preparation methods to produce our samples. It is important to point out that there is no signal from silica defects. We can also observe that the sample annealed in Ar gas (black dashed curve) increases its PL emission after reannealing in RA (blue dotted curve, method B), but this increment remains significantly smaller than the observed for the sample annealed in RA at 1100°C (red solid curve, method A). These results could be explained considering that, after Si ion implantation, the silica matrix is damaged so that, when the sample is annealed at 1100°C in RA, the hydrogen and nitrogen can enhance its diffusion into the matrix, and the nonradiative surface defects on Si-NCs are eliminated. On the other hand, when the sample is annealed in Ar gas at 1100°C, Si-NCs are formed, but the radiation damage is annealed, then the hydrogen diffusion into the silica matrix decreases. So when the sample is annealed at 510°C in RA the hydrogen diffusion is smaller than in a damaged matrix. Therefore, a sample annealed at 1100°C in RA has a more efficient passivation than a sample annealed in Ar gas (and then in RA at 510°C), and consequently its PL emission is higher. Hence, even though the method B appears to be more complex since it is a two-step process, it cannot overcome the PL intensity obtained by the method A, which is simpler and more effective, as we clearly see in the results showed in Figure 1(a). In the following, we will only use the method A to prepare Si-NCs inside a silica matrix and will study other ways to improve its PL intensity.

A sample prepared by method A, and then annealed for 1 h in reducing atmosphere at 1100°C (sample A1), can increase even more its PL (about 30%). Furthermore, its peak value is red shifted as we can see in Figure 1(b) (green dotted curve). The red solid curve (sample A) is shown for comparison. These results have been observed before in samples annealed in RA for more than 1 h [8]. More annealing time at high temperature allows that more hydrogen or nitrogen can

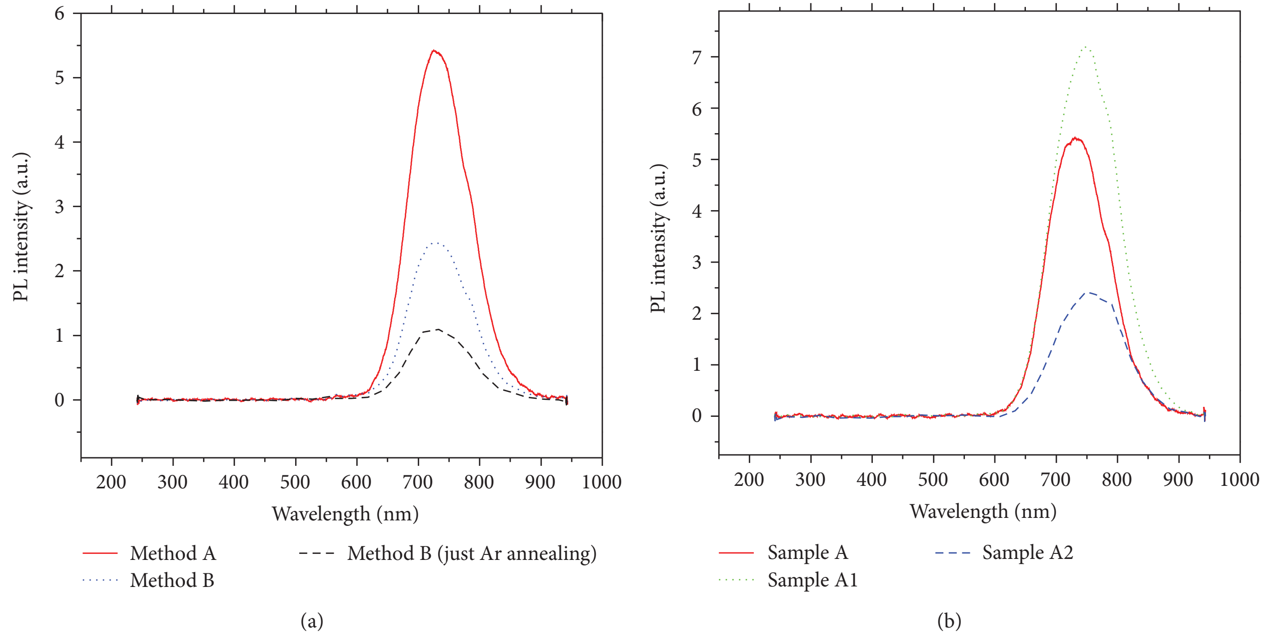

Figure 1: (a) PL emission of samples is annealed at 1100°C for 1 h in reducing atmosphere (red solid curve), and in Ar gas (black dashed curve), and then is annealed at 510°C in reducing atmosphere (blue dotted curve). (b) PL from a sample is annealed at 1100°C in reducing atmosphere for 1 h (red solid curve) and then for 1 h (green dotted curve) and 2 h (blue dashed curve). The excitation wavelength was 250 nm.

diffuse into the matrix. Consequently, more surface defects on Si-NCs are passivated, and their PL signal is higher. But if we continue heating in RA at 1100° for 2 h this sample, A, the PL shows a decrease as shown in Figure 1(b) (blue dashed curve). Also its PL red shift is greater and suggests that the average size of the luminescence Si-NCs has increased. The PL intensity from Si-NCs is size dependent; that is, the largest the nanocrystals are the lower their PL efficiency will be [21, 22]. This effect can explain the decrease in the PL signal when the sample is annealed for more than 2 h at 1100°C. Moreover, once the silica matrix has been restored, the diffusion of hydrogen or nitrogen can decrease, and a depassivation process begins to be dominant. As a consequence of hydrogen desorption, a significant number of surface defects on Si-NCs could reappear. Thus, PL intensity from the system of Si-NCs could decrease even more [6].

Figure 2(a) shows that the PL from a sample with Si-NCs (synthesized by method A), after Ag ion implantation at 1 MeV, is then annealed at 600°C in RA for 1 h. Similar results are showed in Figure 2(b) but now by using Au ion implantation at 1.9 MeV, and heating at 600°C in RA for 1 h. The inset (a1) and (b1) shows the ion range of the implanted materials for the sample implanted with Ag ions and Au ions, respectively. For the implantation with Ag the PL signal has increased almost 4 times (red solid curve) compared to a reference sample (black dashed curve). The PL peak is also blue shifted (~10 nm). The inset (a2) in Figure 2 shows the Ag nanoparticle absorption band in the sample A(Ag). Similar results can be obtained if Au ions are implanted in a sample that contains Si-NCs, as we can see in Figure 2(b). However, the inset b2 shows that there are not any Au NPs formed in the sample since the characteristic plasmon band is not present.

The Ag-implanted ions can form Ag-NPs under a heating treatment at 600°C in RA. So the presence of these NPs could produce a plasmonic interaction of some Ag NPs close to some Si-NCs. In order to check this hypothesis we have prepared similar sample with Ag NPs but now nucleated under Ar atmosphere. Hence, additional passivation of surface defects on Si-NCs could not take place. In Figure 3(a) we can see the PL signal from a sample implanted with Ag ions and annealed at 600°C in Ar gas (sample A2(Ag)-2). A second sample, also implanted with Ag ions, was annealed in RA (sample A2(Ag)-1), as we have done before. In both samples Ag NPs are formed as the inset in Figure 3(a) shows. The sample annealed in Ar gas does not show a significant increase in its PL, while the sample annealed in RA shows the same increment that presented the sample A(Ag). From these results we can deduce that Ag NPs formed into the sample do not have significant plasmonic effect over the PL signal from Si NCs.

Figure 3(b) shows the PL of a sample implanted with Au ions, as explained previously, but annealed in RA at 1100°C for 1 h (sample A(Au)-2). Though the sample A(Au)-2 has Au NPs, as the absorption band shows, the PL from this sample increases but remains smaller than the sample annealed at 600°C in AR during 1 hr (sample(Au)-1), where there are not any Au NPs formed. Therefore, we can conclude that the presence of metal nanoparticles in these systems has not any appreciable plasmonic effect over the PL emission of Si-NCs.

In order to get more insight about the origin of the PL enhancement from Si-NCs in the samples with Ag (or Au) ion implantation, studies of PL intensity in function of excitation photon fluence and time resolved photoluminescence were carried out. The saturation curve allows to obtain

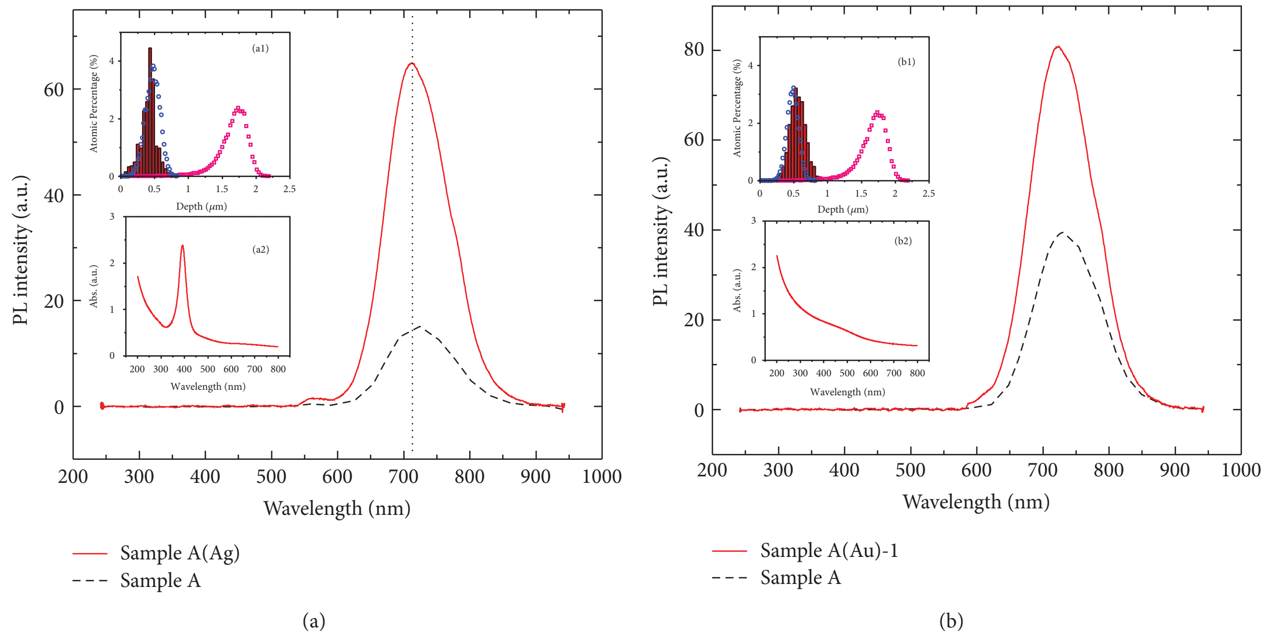

Figure 2: (a) Typical PL emission from a sample containing Si-NCs (sample A) and Si-NCs and Ag NPs (sample A(Ag)). The inset (a1) shows a SRIM simulation of the Ag (blue circles) and Si (pink squares) implanted materials at 1 and 1.5 MeV, respectively. The inset (a2) shows the absorption spectra for the sample with Ag NPs (sample A(Ag)), (b) PL emission from a sample containing Si-NCs (sample A) and Si-NCs and Au NPs (sample A(Au)-1). The inset (b1) shows a SRIM simulation of the Au (blue circles) and Si (pink squares) implanted material at 1.9 and 1.5 MeV, respectively. The inset (b2) shows the absorption spectra for the sample with Au implantation (sample A(Au)-1). The bar graph in (a1) and (b1) is the concentration profile of the implanted ions calculated from RBS measures. The ion fluencies obtained are 5.75×10^{16} atoms/cm^2 and 6.03×10^{16} atoms/cm^2 for the sample with Ag and Au, respectively. In both cases, the excitation wavelength was 355 nm.

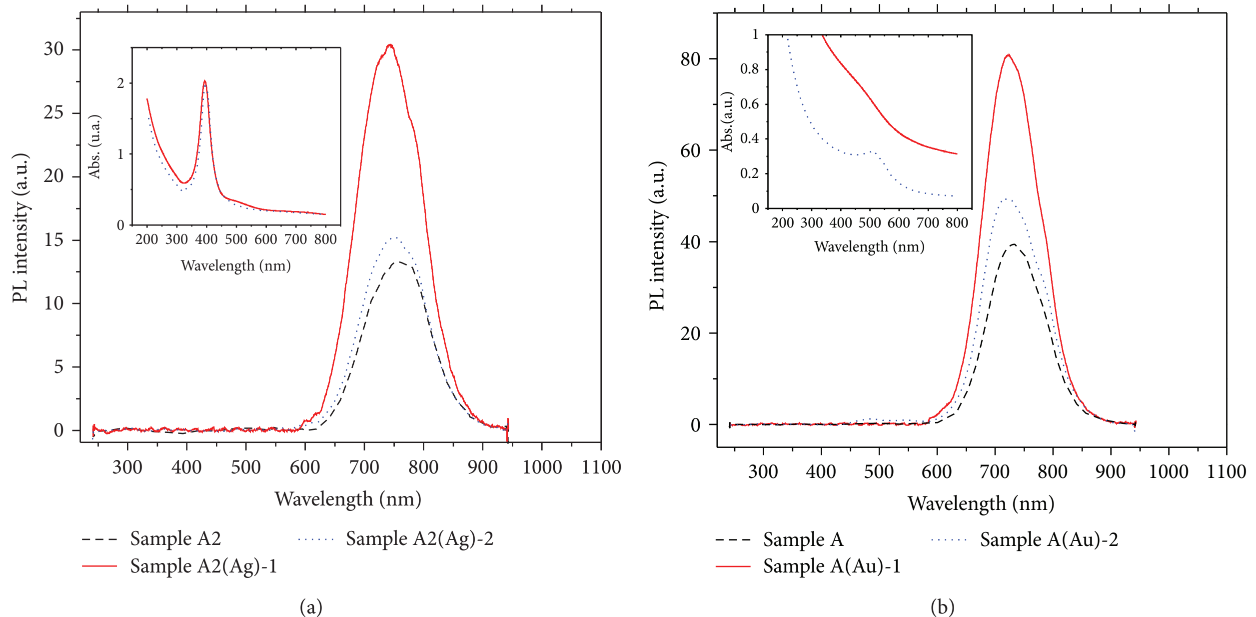

Figure 3: (a) PL emission spectra from samples with Si-NCs and 1 MeV Ag ion implantation, annealed in reducing atmosphere (red solid curve) and Ar atmosphere (blue dotted curve). The black dashed curve is the spectra of the reference sample (only Si-NCs). The excitation wavelength was 355 nm. The inset shows the absorption spectra of the sample with Ag ion implantation after thermal annealing, (b) PL emission from samples with Si-NCs in SiO_2 (black dashed curve) and then with Au ion implantation is annealed in reducing atmosphere at 1100°C (blue dotted curve) or 600°C (red solid curve). The inset shows the absorption spectra of the sample with Au implantation after thermal annealing.

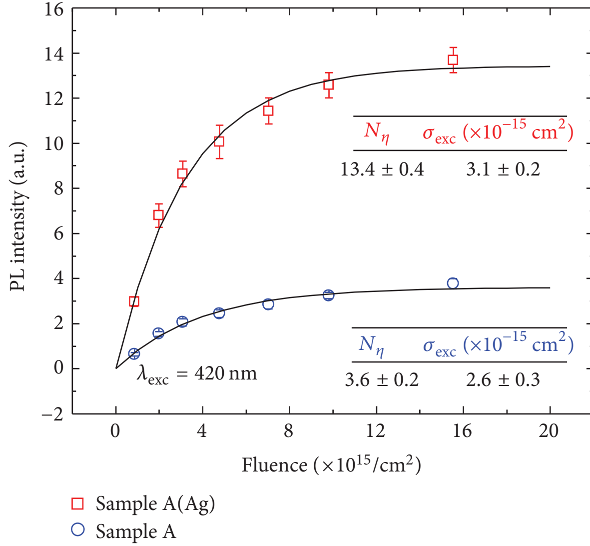

(a)

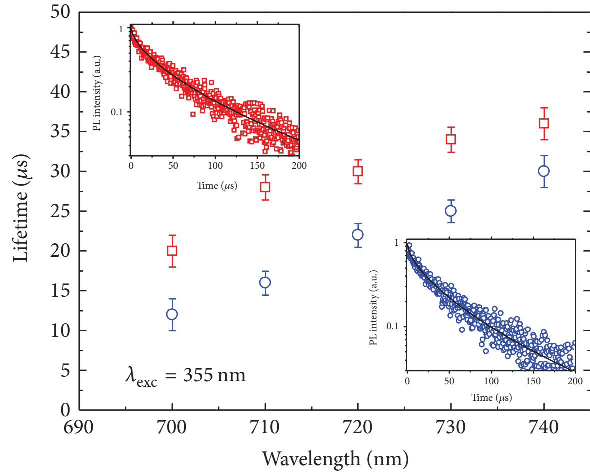

(b)

Figure 4: (a) PL saturation curve for a sample with Si-NCs embedded in silica (blue circles) and with Si-NCs and Ag NPs (red squares), (b) lifetime PL for a set of emission wavelengths. The insets show a typical PL decay curve for sample A (upper left) and sample A(Ag) (lower right).

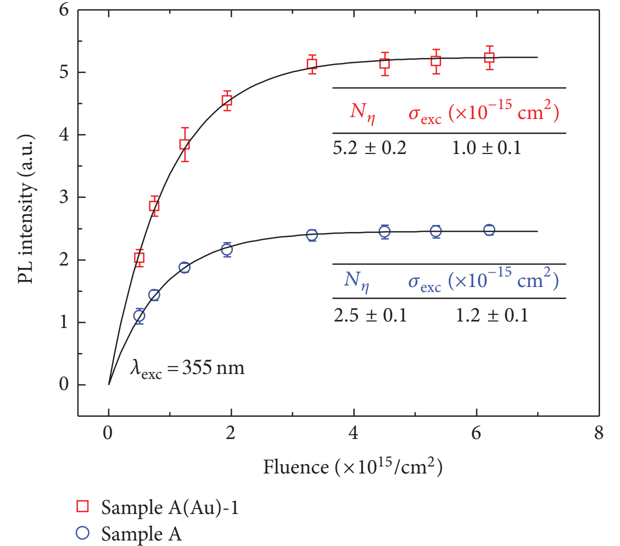

(a)

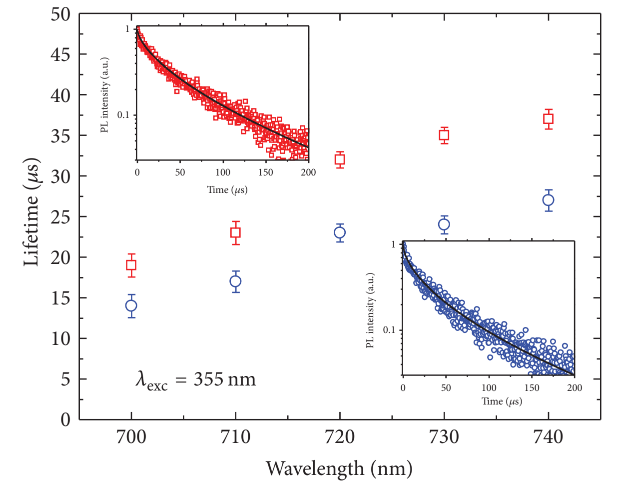

(b)

Figure 5: (a) PL saturation curve for a sample with Si-NCs embedded in silica (blue circles) and with Si-NCs and Au NPs (red squares), (b) lifetime PL for a set of emission wavelength. The insets shows a typical PL decay curve for sample A (upper left) and sample A(Au) 1 (lower right).

the amplification factor of the PL near the saturated pump-power regime in the sample containing Ag NPs (or Au-NPs) where, as we shall see, the PL intensity is limited by the quantum efficiency of the emitters and the total numbers of them. Typical PL emission saturation curves in function of the photon fluence are shown in Figures 4(a) and 5(a) for samples with Ag or Au NPs, respectively. For the sample with Ag, we use 420 nm as excitation wavelength, that is, near the absorption band of Ag-NPs. The emission of Si-NCs is saturated at high photon fluence excitation. By using a two levels model [23–25], the experimental data can be fitted with the theoretical curve given by the fitting equation:

$$I_{em} = N\eta\left(1 - e^{-\sigma_{exc}\Phi}\right), \qquad (1)$$

where N is the total number of Si-NCs that can be excited by the incident beam, η is their PL quantum efficiency, and σ_{exc} is the Si-NCs excitation cross section. From this equation, it can be seen that for large fluencies (Φ tending to infinitum), the saturation level is given by $N\eta$, that is, by the total number of excitable NCs times their PL quantum efficiency.

In the low pump-power regime, we can observe a slight difference between the samples with Ag and Au NPs. The amplification factor obtained at low pump-power in Figure 4(a), for the sample with Ag implantation, is greater than at high fluence. This is reflected by the σ_{exc} value obtained by fitting the experimental data, which is greater in the sample with Ag-NPs than that in the sample without them. On the other hand, Figure 5(a) shows the PL saturation

curve of the sample with Au-implanted ions (sample A(Au)-1). This shows that both samples, one with Au-implanted ions and the other without them, have a similar σ_{exc}. In consequence, the PL amplification factor is similar in both pump-powers regimes. The same results are observed in (sample A(Au)-2), not shown here. The differences observed at low pump-power regime could be explained considering that the layer containing Ag NPs reflects a fraction of the laser excitation light. These laser reflections could increase the effective pump-power over the Si-NCs. To avoid these effects it is convenient to obtain the amplification factor (ΔI_{em}) of PL near the saturated pump power regime as the quotient between the PL intensity of a sample with metal ion implantation ($I_{SiNCs-MIons}$), and one without it (I_{SiNCs}). The factors $\Delta I_{em-Ag\,Ions} \sim 3.7$ and $\Delta I_{em-Au\,Ions} \sim 2.1$ in the pump-power-saturated regimen could be obtained from the results in Figures 4(a) and 5(a).

Figures 4(b) and 5(b) show the values of PL lifetime decay ($\tau_{PL} = \tau_R + \tau_{NR}$) from sample A, A(Ag), and A(Au)-1 taken for a set of emission wavelengths. The insets in these figures show a typical nonexponential decay curve of Si-NCs [26, 27]. For all emission wavelengths the stretching parameter was between 0.6 and 0.7. The increment of luminescence lifetime observed in samples A(Ag) and A(Au)-1 can only be explained if we assume that Si-NCs nonradiative recombination rate has diminished as have been observed in other works [3–6, 8]. This means that the nonradiative lifetime has increased.

The nonradiative state defect can be eliminated using hydrogen, nitrogen, or oxygen to passivate surface defects on Si-NCs, such as the dangling bonds defects known as P_b centers [1, 3–6, 8, 9]. The P_b centers produce a fast nonradiative trap that can be passivated by hydrogen. Moreover, it has been shown that one P_b center is sufficient to quench the luminescence of silicon nanocrystals [4–6, 28]. Then, when the sample A(Ag) is annealed at 600°C in RA, many silicon nanocrystals could reduce the nonradiative decay channels and, consequently, increase their PL quantum efficiency. Other nanocrystals could be activated to emit light such that the number N of nanocrystals which are able to emit increases. From PL lifetime measurements, we can estimate the increment in the PL quantum efficiency ($\Delta\eta$) using its definition in terms of radiative and nonradiative lifetime $\eta = \tau_{PL}/\tau_R$. Taking into account that we have not any evidence of plasmonics effects as a result of the presence of Ag (or Au) nanoparticles in the sample, we can assume that the radiative decay rate does not change, that is, $\Delta\tau_R \sim 1$, for the samples with metal ion implantation. Then, we can obtain the change in PL quantum efficiency as $\Delta\eta_{M\,Ions} = \tau_{PL(SiNCs-M\,Ions)}/\tau_{PL(SiNCs)}$, that is, as the quotient between the measured τ_{PL} for samples with metal ion implantation and the measured for its reference, that is, without metal ion implantation. The increments in the PL quantum efficiency are $\Delta\eta_{Ag\,Ions} \sim 2$ at 710 nm emission wavelength and $\Delta\eta_{Au\,Ions} \sim 1.4$ at 720 nm emission wavelength, as we can obtain from the results of Figures 4(b) and 5(b), respectively. Then the PL quantum efficiency of the systems has an increment about 100% and 40% after Ag or Au ion implantation, respectively.

The increment of the number of Si-NCs optically active can be obtained considering that at high excitation fluence, that is, near the saturated pump-power regime, the PL intensity only depends on the PL quantum efficiency and the total number of Si-NCs optically active. Then it follows that

$$\Delta I_{em} = \Delta N_{M\,Ions} \Delta\eta_{M\,Ions}. \quad (2)$$

Here, $\Delta N_{M\,Ions} = N_{SiNCs-M\,Ions}/N_{SiNCs}$ is the increment in the number of Si-NCs optically active. According to the expression previously mentioned, the number of Si-NCs optically active has an increment about 85% in the sample with Ag ion implantation ($\Delta N_{Ag\,Ions} \sim 1.85$) and about 54% in the sample with Au ion implantation ($\Delta N_{Au\,Ions} \sim 1.54$).

The differences observed in the sample containing Ag with respect to the sample containing Au could be explained by the difficulties to measure the Si implantation real fluence in SiO_2. Thus, probably, the sample A(Ag) has a greater Si implantation fluence than sample A(Au)-1. That slight dissimilarity could produce a greater number of Si-NCs in sample A(Ag) than in sample A(Au)-1. Consequently, the total number of surface defects in each sample could be different. Higher number of Si-NCs means a greater total number of surface defects P_b to be passivated. So the sample with a higher number of Si-NCs, that is, higher Si real fluence, will have the possibility to increase its PL efficiency even more than a sample with a lower number of them.

4. Conclusions

We have synthesized a system of Si-NCs embedded in silica at high depth inside the matrix (1-2 μm). We observed that the annealing of the Si-ion-implanted silica in RA at 1100°C for 1 h is the best method to obtain a system of Si-NCs with high PL intensity. In addition, thermal annealing for more than one hour in reducing atmosphere can increase the PL signal during the first hour with about 30%. However, more than two hours under these annealing conditions produce a decrease in the PL signal, and the spectra are shifted toward the infrared. On the other hand, we have found a method to amplify the PL signal from a sample containing Si-NCs by means of ion metal implantation (Ag or Au) and a second annealing treatment in RA at 600°C. This method produces a fourfold PL signal enhancement for the case of using Ag ions (or twofold PL signal enhancement using Au ions). This PL enhancement is far greater than we can obtain by a second thermal annealing (at 1100°C or 600°C, for more than 1 h in RA) without metal ion implantation. The ion-metal-implantation-induced damage can increase the amount of hydrogen, or nitrogen, which diffuses into the silica matrix. As a consequence, we achieve a better passivation of the Si-NCs system. This passivation process, assisted by metal ion implantation, increases the PL quantum efficiency and the number of Si-NCs optically active of the system. Though Si-NCs are embedded at high depth under the silica surface, the ion metal implantation process, together with proper thermal annealing, proves to be an efficient way to passivate surface defects on it. As a result, we have a robust and efficiently passivated system of Si-NCs. This system is better

protected from external damage and contamination and could be used for application in light emitter silicon based for optoelectronic devices.

Acknowledgments

The authors express their thanks to Karim López and Francisco Jaimes for running the accelerator and J. G. Morales for his assistance during the samples preparation. This work was partially funded by DGAPA-UNAM, with Project no. IN108412 and IN108510 and by CONACyT with project 102937. Nonlinear optics laboratory acknowledges partial financial support from AFOSR-FA9550-12-1-0235 Grant. J. Bornacelli acknowledges financial support by CONACyT through Scholarship 216107.

References

[1] B. G. Fernandez, M. López, C. García et al., "Influence of average size and interface passivation on the spectral emission of Si nanocrystals embedded in SiO_2," *Journal of Applied Physics*, vol. 91, no. 2, pp. 798–807, 2002.

[2] M. L. Brongersma, A. Polman, K. S. Min, E. Boer, T. Tambo, and H. A. Atwater, "Tuning the emission wavelength of Si nanocrystals in SiO_2 by oxidation," *Applied Physics Letters*, vol. 72, no. 20, pp. 2577–2579, 1998.

[3] M. López, B. Garrido, C. García et al., "Elucidation of the surface passivation role on the photoluminescence emission yield of silicon nanocrystals embedded in SiO_2," *Applied Physics Letters*, vol. 80, no. 9, pp. 1637–1639, 2002.

[4] A. R. Wilkinson and R. G. Elliman, "Passivation of Si nanocrystals in SiO_2: atomic versus molecular hydrogen," *Applied Physics Letters*, vol. 83, no. 26, pp. 5512–5514, 2003.

[5] R. Lockwood, S. McFarlane, J. R. Rodríguez Núñez, X. Y. Wang, J. G. C. Veinot, and A. Meldrum, "Photoactivation of silicon quantum dots," *Journal of Luminescence*, vol. 131, no. 11, pp. 1530–1535, 2011.

[6] A. R. Wilkinson and R. G. Elliman, "Kinetic of H_2 passivation of Si nanocrystals in SiO_2," *Physical Review B*, vol. 68, Article ID 155302, 2003.

[7] D. Jurbergs, E. Rogojina, L. Mangolini, and U. Kortshagen, "Silicon nanocrystals with ensemble quantum yields exceeding 60%," *Applied Physics Letters*, vol. 88, no. 23, Article ID 233116, 2006.

[8] A. R. Wilkinson and R. G. Elliman, "The effect of annealing environment on the luminescence of silicon nanocrystals in silica," *Journal of Applied Physics*, vol. 96, no. 7, pp. 4018–4020, 2004.

[9] M. Bolduc, G. Genard, M. Yedji et al., "Influence of nitrogen on the growth and luminescence of silicon nanocrystals embedded in silica," *Journal of Applied Physics*, vol. 105, no. 1, Article ID 013108, 2009.

[10] J. S. Biteen, D. Pacifici, N. S. Lewis, and H. A. Atwater, "Enhanced radiative emission rate and quantum efficiency in coupled silicon nanocrystal-nanostructured gold emitters," *Nano Letters*, vol. 5, no. 9, pp. 1768–1773, 2005.

[11] T. Shimizu-Iwayama, T. Hama, D. E. Hole, and I. W. Boyd, "Characteristic photoluminescence properties of Si nanocrystals in SiO_2 fabricated by ion implantation and annealing," *Solid-State Electronics*, vol. 45, no. 8, pp. 1487–1494, 2001.

[12] A. L. Tchebotareva, M. J. A. de Dood, J. S. Biteen, H. A. Atwater, and A. Polman, "Quenching of Si nanocrystal photoluminescence by doping with gold or phosphorous," *Journal of Luminescence*, vol. 114, no. 2, pp. 137–144, 2005.

[13] A. N. Mikhaylov, A. B. Kostyuk, D. S. Korolev et al., "Formation of gold nanoparticles in single-layer and multi-layer ensembles of light-emitting silicon nanocrystals using ion implantation," *Bulletin of the Russian Academy of Sciences: Physics*, vol. 76, no. 2, pp. 214–217, 2012.

[14] A. K. Singh, K. G. Gryczynski, S. Y. Park, M. Kim, and A. Neogi, "Broad band light emission from Ag-ion implanted silicon nanocrystals," *Solid State Communications*, vol. 151, pp. 1405–1409, 2011.

[15] A. K. Singh, K. G. Gryczynski, and A. Neogi, "Origin of room temperature broadband light emission and carrier dynamics in Ag ion-implanted Silicon nanocrystals," *Optical Material Express*, vol. 2, no. 5, pp. 501–509, 2012.

[16] H. Mertens, J. S. Biteen, H. A. Atwater, and A. Polman, "Polarization-selective plasmon-enhanced silicon quantum-dot luminescence," *Nano Letters*, vol. 6, no. 11, pp. 2622–2625, 2006.

[17] A. Oliver, J. A. Reyes-Esqueda, J. C. Cheang-Wong et al., "Controlled anisotropic deformation of Ag nanoparticles by Si ion irradiation," *Physical Review B*, vol. 74, Article ID 245425, 6 pages, 2006.

[18] A. Oliver, J. C. Cheang-Wong, A. Crespo et al., "E' and B_2 center production in amorphous quartz by MeV Si and Au ion implantation," *Materials Science and Engineering B*, vol. 78, pp. 32–38, 2000.

[19] M. Watanabe, S. Juodkazis, H. B. Sun, S. Matsuo, and H. Misawa, "Luminescence and defect formation by visible and near-infrared irradiation of vitreous silica," *Physical Review B*, vol. 60, no. 14, pp. 9959–9964, 1999.

[20] L. Skuja, M. Hirano, H. Hosono, and K. Kajihara, "Defects in oxide glasses," *Physica Status Solidi (C)*, vol. 2, no. 1, pp. 15–24, 2005.

[21] S. P. Withrow, C. W. White, A. Meldrum, J. D. Budain, D. M. Humbree Jr., and J. C. Barbour, "Effects of hydrogen in the annealing environment on photoluminescence from Si nanoparticles in SiO_2," *Journal of Applied Physics*, vol. 86, no. 1, pp. 396–401, 1999.

[22] T. Shimizu-Iwayama, K. Fujita, S. Nakao, K. Saitoh, T. Fujita, and N. Itoh, "Visible photoluminescence in Si^+-implanted silica glass," *Journal of Applied Physics*, vol. 75, no. 12, pp. 7779–7783, 1994.

[23] M. Wojdak, M. Klik, M. Forcales et al., "Sensitization of Er luminescence by Si nanoclusters," *Physical Review B*, vol. 69, no. 23, Article ID 233315, 2004.

[24] D. Kovalev, J. Diener, H. Heckler, G. Polisski, N. Künzner, and F. Koch, "Optical absorption cross sections of Si nanocrystals," *Physical Review B*, vol. 61, no. 7, pp. 4485–4487, 2000.

[25] D. Timmerman, I. Izeddin, and T. Gregorkiewicz, "Saturation of luminescence from Si nanocrystals embedded in SiO_2," *Physica Status Solidi (A)*, vol. 207, no. 1, pp. 183–187, 2010.

[26] J. Linnros, N. Lalic, A. Galeckas, and V. Grivickas, "Analysis of the stretched exponential photoluminescence decay from nanometer-sized silicon crystals in SiO_2," *Journal of Applied Physics*, vol. 86, no. 11, pp. 6128–6134, 1999.

[27] O. Guillois, N. Herlin-Boime, C. Reynaud, G. Ledoux, and F. Huisken, “Photoluminescence decay dynamics of noninteracting silicon nanocrystals,” *Journal of Applied Physics*, vol. 95, no. 7, pp. 3677–3682, 2004.

[28] M. Lannoo, C. Delerue, and G. Allan, “Theory of radiative and nonradiative transitions for semiconductor nanocrystals,” *Journal of Luminescence*, vol. 70, no. 1–6, pp. 170–184, 1996.

Journal of
Nanotechnology

International Journal of
Corrosion

International Journal of
Polymer Science
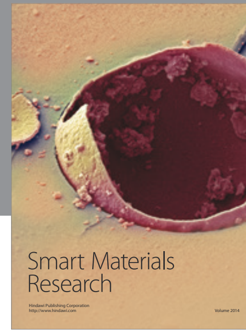
Smart Materials
Research

Journal of
Composites

BioMed
Research International

Hindawi
Submit your manuscripts at
http://www.hindawi.com
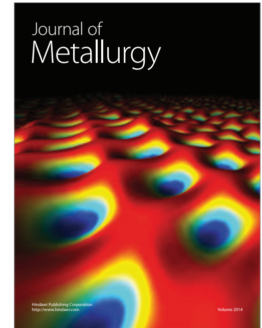
Journal of
Metallurgy

Journal of
Materials
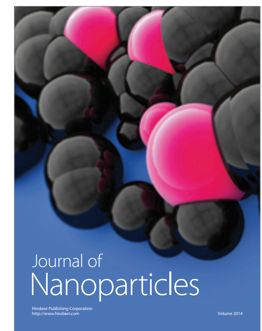
Journal of
Nanoparticles
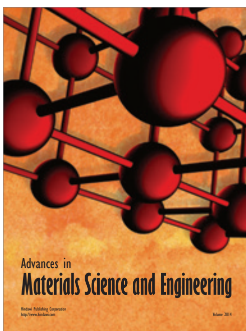
Advances in
Materials Science and Engineering
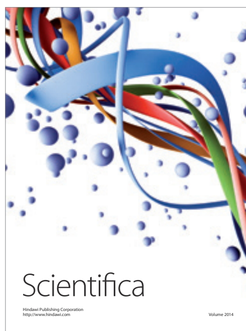
Scientifica
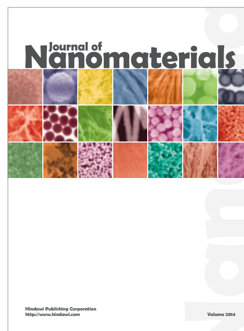
Journal of
Nanomaterials
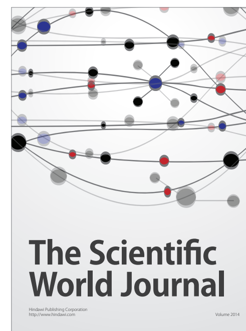
The Scientific
World Journal

International Journal of
Biomaterials

Journal of
Nanoscience

Journal of
Coatings

Journal of
Crystallography

Journal of
Ceramics

Journal of
Textiles